Selective enhancement of topologically induced interface states

Charles Poli, Matthieu Bellec, Ulrich Kuhl, Fabrice Mortessagne, Henning Schomerus

Selective enhancement of topologically induced interface states

Charles Poli,[1] Matthieu Bellec,[2] Ulrich Kuhl,[2]
Fabrice Mortessagne,[2] and Henning Schomerus*[1]

[1]*Department of Physics, Lancaster University, Lancaster, LA1 4YB, United Kingdom*

[2]*Laboratoire de Physique de la Matière Condensée, CNRS UMR 7336, Université Nice Sophia Antipolis, 06100 Nice, France*

Abstract

The recent realization of topological phases in insulators and superconductors has raised the prospects to advance robust quantum technologies. The desire to demonstrate the underlying topological features with a high level of control has given incentive to explore optical platforms for analogous realizations. Here we show that the functionality of optical systems can be enhanced by combining topological protection with non-hermitian symmetries that do not have an electronic counterpart. This is achieved by combining parity-time symmetric losses with a unique feature of topologically induced interface states, namely, that they break a sublattice symmetry. This property isolates the state from the losses and enhances its visibility both in the frequency and in the time domain.

A key ingredient for topological functionality are robust confined states that form at interfaces between regions with topologically distinct band structures. For electromagnetic waves, this can be realized in two dimensions by breaking symmetries in analogy to the quantum Hall effect [1–3] or the quantum spin Hall effect [4–6], while in one dimension one can employ lattice modulations [7–9]. The intrinsic robustness of these topological states raises the question whether they can be controlled and modified independently of the other states in the system. Here, we draw on passive non-hermitian parity-time(PT)-symmetry [10–13] to demonstrate the selective control and enhancement of a topologically induced state in a one-dimensional microwave set-up [14–17]. The state can be isolated from losses affecting all other modes in the system, which enhances its visibility in the temporal evolution of a pulse, even in presence of structural disorder.

A minimal one-dimensional model with a topological band structure is a chain of sites with alternating couplings (*i.e.* a dimer chain). This model was originally introduced in an electronic context by Su, Schrieffer and Heeger (SSH) [18] to describe fractionalized charges in polyacetylene, which appear in the presence of a dimerization defect. Photonic systems provide a versatile platform to realize analogies of this situation. In absence of PT-symmetry, the topological defect state has been observed in a quantum walk scenario [9] while a dimer chain with a non-topological defect has been realised in a wave guide array [19], and the PT-symmetric variant of the chain without a defect has been discussed in [20]. Here, we implement the SSH chain in presence of the defect and PT-symmetry by means of a set of identical coupled dielectric resonators placed in a microwave cavity. Localized absorptive losses enable us to address non-hermitian effects that do not have an electronic analogue.

RESULTS

Realization of dimer chains by coupled disk resonators. Fig. 1a depicts a chain of 21 microwave resonators with a central dimerization defect. We establish a one-dimensional tight-binding regime [14], where the electromagnetic field is mostly confined within the resonators. For an isolated disk, only a single mode is important in a broad spectral range around the bare frequency $\nu_b = 6.65\,\mathrm{GHz}$. This mode spreads out evanescently, so that the coupling strength can be controlled by adjusting the separation distance between the resonators [14]. The resulting system can be described by the following tight-binding equa-

tions:

$$
\begin{array}{ll}
(\alpha) & \begin{cases} (\nu-\nu_n)\psi_n = t_2\psi_{n-1} + t_1\psi_{n+1}, & n=-2,-4,\ldots \\ (\nu-\nu_n)\psi_n = t_1\psi_{n-1} + t_2\psi_{n+1}, & n=-1,-3,\ldots, \end{cases} \\
\text{inter-face} & \begin{cases} (\nu-\nu_0)\psi_0 = t_2(\psi_{-1}+\psi_1), & n=0, \end{cases} \\
(\beta) & \begin{cases} (\nu-\nu_n)\psi_n = t_2\psi_{n-1} + t_1\psi_{n+1}, & n=1,3,\ldots, \\ (\nu-\nu_n)\psi_n = t_1\psi_{n-1} + t_2\psi_{n+1}, & n=2,4,\ldots, \end{cases}
\end{array}
\tag{1}
$$

where n enumerates the resonators, with $n = -10, -9, -8, \ldots 10$ and $n = 0$ for the central site (see Fig. 1b). The mode amplitude in the nth resonator is given by ψ_n, t_1 and t_2 denote the alternating nearest-neighbor coupling strengths, while ν_n is the resonance frequency of the nth isolated resonator. Without absorption, the resonance frequencies are equal to the bare frequency, $\nu_n = \nu_b$. Absorption is introduced on selected sites by depositing elastomer patches on top of the dielectric cylinders (see Fig. 1a). The losses give rise to a complex resonance frequency $\nu_n = \nu_b' - i\gamma$, and also shift the real part of the bare frequency to $\nu_b' \approx \nu_b - \gamma$. In our experiments, $\gamma \simeq 40\,\text{MHz}$, while the separations $d_1 = 12\,\text{mm}$ and $d_2 = 15\,\text{mm}$ correspond to couplings $t_1 = 37.1\,\text{MHz}$ and $t_2 = 14.8\,\text{MHz}$, respectively.

Defect-free chains. As a reference situation, we first consider a defectless SSH chain without absorption. As depicted in Fig. 2a, the density of states (DOS) is characterized by a band structure with two bands separated by a finite gap of size $2|t_1 - t_2| = 45\,\text{MHz}$ (gray zone). The extended states occupy bands in the range $\nu_b - t_1 - t_2 < \nu < \nu_b - |t_1 - t_2|$ and $\nu_b + |t_1 - t_2| < \nu < \nu_b + t_1 + t_2$. The DOS is not affected when the values of the couplings t_1 and t_2 are interchanged. Nevertheless, a topological distinction between these two situations (called hereafter α and β configurations) can be captured by a winding number associated to the Bloch wave functions (see [21, 22] and Supplementary Section S.1). An interface between both configurations takes the form of a dimerization defect where two consecutive couplings are identical (red zone in Fig. 1b and Fig. 2b). The topological distinctiveness of the two phases leads to the formation of an exponentially localized midgap state at $\nu = \nu_b$. The corresponding wavefunction can be read off from equation (1), and takes the form $\psi_n = (-t_1/t_2)^{-|n|/2}$ for even n and $\psi_n = 0$ for odd n. The midgap state is therefore confined to the sublattice with even index, which we will call the A-sublattice, while the sites with odd index are called the B-sublattice. The complementary state on the B-sublattice increases

exponentially and is incompatible with the boundary conditions.

Dimerization defect. Fig. 2b shows the DOS measured for a 21-resonator SSH chain with a central dimerization defect, still without absorption. Twenty-one modes are observed within the spectral range of interest. Of these, 20 modes are extended over the whole system. These modes group into two sets of 10 and correspond to the upper and the lower band of the infinite dimer chain. The bands remain separated by a 45 MHz gap. The topologically induced mode clearly sits the middle of the gap, at frequency ν_b. We find that the intensity of the midgap state belonging to the B-sublattice is zero within experimental resolution, and thus confirm that the wavefunction is confined to the A-sublattice. The corresponding wavefunction intensity profile pertaining to the A sites is depicted in Fig. 2d (red dots). As expected, the intensity decays according to an exponential profile given by the theoretical result (shown in gray).

Selective enhancement. We now set out to enhance the visibility of the topologically induced state. Our approach rests on the realization that the topological features of the system extend to a staggered configuration of losses, obtained by depositing absorptive material on all B sites [22]. Both in the α and in the β configuration, the tight-binding system then still possesses a passive $(\mathcal{PT})$-symmetry, given by a reflection $(\mathcal{P})$ at a point in the middle of a dimer, which maps the passive A sites onto the lossy B sites but leaves the couplings unchanged. This mapping corresponds to a time-reversal operation $(\mathcal{T})$ up to a constant complex frequency shift $i\gamma$. As a consequence of this symmetry, all extended states are uniformly suppressed by the losses (their complex resonance frequencies all acquire the same imaginary part $-\gamma/2$), while the topologically induced interface state remains pinned at $\nu = \nu_b$ and thus is unaffected by the losses (see Supplementary Section S.1).

The spectral analysis presented in Fig. 2c shows that the extended modes shift downwards in frequency and become broadened, while the overall spectral weight in the resulting continuous bands is reduced. These features are consistent with the frequency dressing on the B sites, $\nu_b \to \nu_b - \gamma - i\gamma$. In contrast, the peak in the density of states associated to the zero-mode remains fixed at the bare frequency ν_b, and its height and width is almost unchanged. As shown in Fig. 2e this mode remains well confined to the A-sublattice, and still displays an exponential intensity profile as one moves away from the defect site. (Under the same conditions *non-topological* defect states hybridize, thereby degrading their properties, see Supplementary Section S.2.)

The spectral analysis implies that the interface state is insensitive to the losses distributed on the B sites. It then should become the predominant mode during the time evolution. To illustrate this feature, Fig. 3 shows the time evolution for both non-absorptive (a) and absorptive (b) cases, corresponding to a pulse launched on the defect site. Without absorption, diffraction and interferences spoil the propagation of the interface state, which cannot be discerned after 250 ns. On the contrary, adding losses drastically enhances the visibility of the topologically induced mode, which then dominates the propagation without any degradation.

Robustness against structural disorder. To probe the topological protection property of the midgap state, we introduce structural disorder by randomly distributing the intersite separations. In the tight-binding description, this corresponds to a random modification of the coupling strengths. We preserve the dimer structure by defining the couplings as $t^r_{1,2} = \tilde{t}_{1,2} + \tilde{t}(W/2)\xi$, where $\tilde{t}_1 = (3t_1 + t_2)/4 = 31.5\,\mathrm{MHz}$, $\tilde{t}_2 = (t_1 + 3t_2)/4 = 20.4\,\mathrm{MHz}$ and $\tilde{t} = (t_1 - t_2)/2 = 11.1\,\mathrm{MHz}$. Here W is the disorder strength varying from 0 to 0.95 and ξ is a random number uniformly distributed in the interval [-1, 1] (see Fig. 4a). As shown in Fig. 4b, for different values of W the zero-mode intensities exhibit a very similar profile: an approximately exponential decay on the A sites and insignificant intensity on the B sites. Even though we do not perform any averaging over disorder realizations, the experimental profile is in remarkable agreement with the simple exponential $(\tilde{t}_1/\tilde{t}_2)^{-|n|}$. Note that as $\tilde{t}_1/\tilde{t}_2 = 1.54 < t_1/t_2 = 2.51$ the present zero-modes are more extended compared to the situation considered previously (Fig. 2d). When absorption is added on B sites, we observe in Fig. 4c that the robustness of the mode persists. Due to the resonance frequency shift of the lossy resonators, the couplings are now slightly changed to an effective coupling ratio $(\tilde{t}_1/\tilde{t}_2)_{\mathrm{eff}} = 1.92$, which is taken into account in the theoretical profile (gray shaded curve).

DISCUSSION

The loss-induced selective enhancement of the topological interface state observed in this work exploits the unique structure of the zero-mode wavefunction, which is confined to a sublattice. Such sublattice-symmetry breaking is common in topologically induced states; for example, it also occurs for the 0th Landau level in the quantum Hall effect of massless relativistic particles [23], as well as in inhomogeneously strained graphene [24] and

photonic analogues of deformed honeycomb lattices [25, 26]. The combination of topological constraints and passive ($\mathcal{PT}$)-symmetry therefore provides a generic concept which may be exploited in different settings. This also extends to atom-optical systems, where the defectless version of the passive SSH model has recently been realized in an optical lattice [27], while the nonpassive case has been discussed in theoretical work [28]. We note that it is also possible to selectively suppress the interface state, which can be achieved either by placing the losses on the other sublattice or by interchanging the couplings (topological phases) on both sides of the defect. The enhancement or suppression of the state can therefore be used to detect the relative size of two coupling strengths. It is also attractive to replace the losses by amplification, *e.g.* in a layered structure of materials with different thickness, which could be used to realize a laser with a much simplified mode competition, or by nonlinear effects as occurring *e.g.* in chains of coupled quantum dot or quantum well exciton polaritons [29].

METHODS

Microwave realization of tight-binding systems. The experimental setup and the tight-binding description of the microwave system are detailed in [14]. We describe the main ingredients. The sites of the lattice are occupied by dielectric microwave resonators with a cylindrical shape (5 mm height, 8 mm diameter, and a refractive index of 6). The resonance frequency of an isolated resonator ν_b is around 6.65 GHz and corresponds to the on-site energy of atoms in a tight-binding model. The dielectric cylinders are coupled by the evanescent electromagnetic field, the corresponding coupling strength t between two resonators is well described by a tight-binding-like hopping term; t depends on the separation d between resonators. Via a reflection measurement, one has access, at each site, to the local density of states and to the wavefunction intensity associated to each eigenfrequency. The density of states (DOS) is obtained by averaging the local density of states over all resonator positions. To obtain the time evolution of the pulse we measure the transmission between a source located at the interface site and a receiver successively placed at each site position. By performing a Fourier transform, one obtains the temporal evolution of a pulse initiating from the defect site and propagating into the SSH chain. In all these experiments, we face an intrinsic on-site disorder of $\sim 0.15\%$ in the values of ν_b.

[1] Wang, Z., Chong, Y. Joannopoulos, J. D. & Soljačić, M. Observation of unidirectional backscattering-immune topological electromagnetic states. *Nature* **461**, 772–775 (2009).

[2] Fang, K., Yu, Z. & Fan, S. Realizing effective magnetic field for photons by controlling the phase of dynamic modulation. *Nature Photon.* **6**, 782–787 (2012).

[3] Rechtsman, M. C. *et al.* Photonic Floquet topological insulators. *Nature* **496**, 196–200 (2013).

[4] Hafezi, M., Demler, E. A., Lukin, M. D. & Taylor, J. M. Robust optical delay lines with topological protection. *Nature Phys.* **7**, 907–912 (2011).

[5] Khanikaev, A. B. *et al.* Photonic topological insulators. *Nature Mater.* **12**, 233–239 (2013).

[6] Hafezi, M., Mittal, S., Fan, J., Migdall, A. & Taylor, J. M. Imaging topological edge states in silicon photonics. *Nature Photon.* **7**, 1001–1005 (2013).

[7] Malkova, N., Hromada, I., Wang, X., Bryant, G. & Chen, Z. Observation of optical Shockley-like surface states in photonic superlattices. *Opt. Lett.* **34**, 1633–1635 (2009).

[8] Kraus, Y. E., Lahini, Y., Ringel, Z., Verbin, M. & Zilberberg, O. Topological states and adiabatic pumping in quasicrystals. *Phys. Rev. Lett.* **109**, 106402 (2012).

[9] Kitagawa, T. *et al.* Observation of topologically protected bound states in photonic quantum walks. *Nature Commun.* **3** (2012).

[10] Guo, A. *et al.* Observation of $\mathcal{PT}$-symmetry breaking in complex optical potentials. *Phys. Rev. Lett.* **103**, 093902 (2009).

[11] Rüter, C. E. *et al.* Observation of parity–time symmetry in optics. *Nature Phys.* **6**, 192–195 (2010).

[12] Feng, L. *et al.* Experimental demonstration of a unidirectional reflectionless parity–time metamaterial at optical frequencies. *Nature Mater.* **12**, 108–113 (2012).

[13] Regensburger, A. *et al.* Parity-time synthetic photonic lattices. *Nature* **488**, 167–171 (2012).

[14] Bellec, M., Kuhl, U., Montambaux, G. & Mortessagne, F. Tight-binding couplings in microwave artificial graphene. *Phys. Rev. B* **88**, 115437 (2013).

[15] Laurent, D., Legrand, O., Sebbah, P., Vanneste, C. & Mortessagne, F. Localized modes in a finite-size open disordered microwave cavity. *Phys. Rev. Lett.* **99**, 253902 (2007).

[16] Bellec, M., Kuhl, U., Montambaux, G. & Mortessagne, F. Topological transition of Dirac points in a microwave experiment. *Phys. Rev. Lett.* **110**, 033902 (2013).

[17] Franco-Villafañe, J. A. *et al.* First experimental realization of the Dirac oscillator. *Phys. Rev. Lett.* **111**, 170405 (2013).

[18] Su, W. P., Schrieffer, J. R. & Heeger, A. J. Solitons in polyacetylene. *Phys. Rev. Lett.* **42**, 1698 (1979).

[19] Keil, R. *et al.* The random mass dirac model and long-range correlations on an integrated optical platform. *Nature Commun.* **4**, 1368– (2013).

[20] Ramezani, H., Christodoulides, D. N., Kovanis, V., Vitebskiy, I. & Kottos, T. $\mathcal{P}t$-symmetric Talbot effect. *Phys. Rev. Lett.* **109**, 033902 (2012).

[21] Ryu, S. & Hatsugai, Y. Topological origin of zero-energy edge states in particle-hole symmetric systems. *Phys. Rev. Lett.* **89**, 077002 (2002).

[22] Schomerus, H. Topologically protected midgap states in complex photonic lattices. *Opt. Lett.* **38**, 1912 (2013).

[23] Jackiw, R. Fractional charge and zero modes for planar systems in a magnetic field. *Phys. Rev. D* **29**, 2375–2377 (1984).

[24] Guinea, F., Katsnelson, M. I. & Geim, A. K. Energy gaps and a zero-field quantum Hall effect in graphene by strain engineering. *Nature Phys.* **6**, 30–33 (2009).

[25] Rechtsman, M. C. *et al.* Strain-induced pseudomagnetic field and photonic Landau levels in dielectric structures. *Nature Photon.* **7**, 153–158 (2013).

[26] Schomerus, H. & Halpern, N. Y. Parity anomaly and Landau-level lasing in strained photonic honeycomb lattices. *Phys. Rev. Lett.* **110**, 013903 (2013).

[27] Atala, M. *et al.* Direct measurement of the Zak phase in topological Bloch bands. *Nature Phys.* **9**, 795–800 (2013).

[28] Barnett, R. Edge-state instabilities of bosons in a topological band. *Phys. Rev. A* **88**, 063631 (2013).

[29] Walker, P. M. *et al.* Exciton polaritons in semiconductor waveguides. *Appl. Phys. Lett.* **102**, 012109 (2013).

Acknowledgments. CP and HS acknowledge support of EPSRC via grant EP/J019585/1.

Author Contributions. CP and HS developed the concept and theory, MB and FM performed the experiments and analyzed the data. All the authors participated in the discussions and in writing the paper.

Competing financial interests. The authors declare no competing financial interests.

FIG. 1. **Complex SSH chain. a.** Picture of the experimental microwave realization of the complex SSH chain. The lattice is composed of 21 identical coupled dielectric cylindrical resonators (5 mm height, 8 mm diameter, and a refractive index of 6) sandwiched between two metallic plates (note that the top plate is not shown). To implement dimer chains, the resonators are separated by d_1 or d_2 with $d_1 < d_2$, *i.e.* coupling $t_1 > t_2$. A central dimerization defect is introduced. The defect creates an interface state at zero energy, a "zero-mode", whose visibility is enhanced by means of absorptive patches placed on one of the two sublattices. The resulting wavefunction intensity is superimposed onto the chain. **b.** Schematic of the complex SSH chain, with A and B-sublattices indicated in white and gray respectively. The strong (weak) coupling strength is represented by a thick (thin) line. In our system, the couplings can be controlled by varying the resonator spacings. The topologically induced zero-mode appears at the interface (red) between α configuration (with strong intradimer coupling) and β configuration (with weak intradimer coupling).

FIG. 2. **Experimental density of states (DOS) and zero-mode profiles of SSH chains with and without absorption. a.** DOS obtained for a defectless SSH chain (no interface, see inset) for separation distances $d_1 = 12\,\mathrm{mm}$ ($t_1 = 37.1\,\mathrm{MHz}$) and $d_2 = 15\,\mathrm{mm}$ ($t_1 = 14.8\,\mathrm{MHz}$). The reference frequency is the bare frequency of an isolated resonator $\nu_b = 6.65\,\mathrm{GHz}$. Two bands separated by a gap (gray zone) are observed. **b.** DOS obtained for a SSH chain with a dimerization defect (inset, red circle). A zero-mode appears in the band gap. **c.** DOS obtained for a complex SSH chain dimerization defect (inset, red circle) and absorption located on B sites (inset, black filled circles). While all the extended modes experience losses, the zero-mode is preserved. (Note that the ordinate axes scales are different). **d.** Experimental (red dots) and theoretical (gray region) intensity profile of the zero-mode on the A sites, for the chain without absorption. The intensity is zero on B-sites, and the total intensity is normalized to unity. **e.** Intensity profile of the zero-mode in presence of losses on B-sites.

FIG. 3. **Selective enhancement of the zero-mode. a.** Time evolution of the field intensity (normalized at each time step) in the SSH chain without absorption when the initial excitation corresponds to the central site (*i.e.* at the interface, red arrow). All modes are participating to the propagation. **b.** Time evolution of the field intensity in the complex SSH chain with absorption on B-sites. The zero-mode is enhanced and control the propagation.

FIG. 4. **Zero-mode robustness against disorder. a.** Schematic of the coupling strengths used in the experiments. The disorder strength W is chosen to preserve the topological structure of the chain (see text). **b.** Zero-mode intensity profiles (normalized to 1) on A sites for the disordered chain without losses for different values of W. The gray shaded curve follows the exponential profile $(\tilde{t}_1/\tilde{t}_2)^{-|n|}$. **c.** Intensity profiles in the presence of losses on the B-sites. The gray shaded curve is calculated for the effective coupling ratio $(\tilde{t}_1/\tilde{t}_2)_{\text{eff}} = 1.92$. The topologically induced interface state is robust against structural disorder with and without absorption.

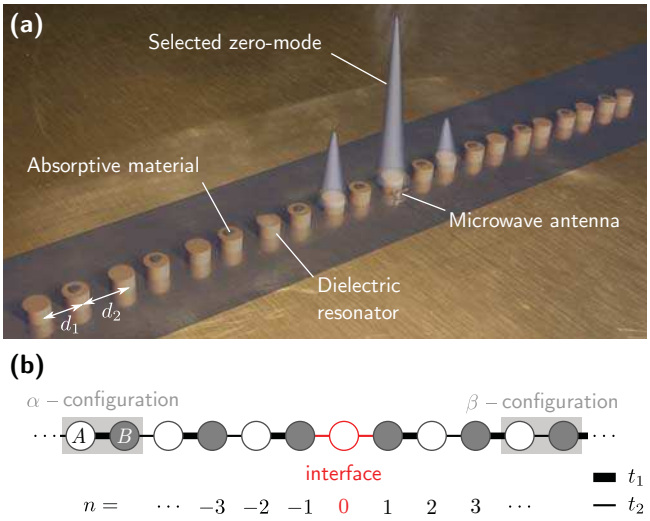
(a)
Selected zero-mode
Absorptive material
Microwave antenna
Dielectric
resonator
d_1
d_2
(b)
α – configuration
β – configuration
A
B
interface
t_1
t_2
$n =$ $\cdots$ -3 -2 -1 0 1 2 3 $\cdots$

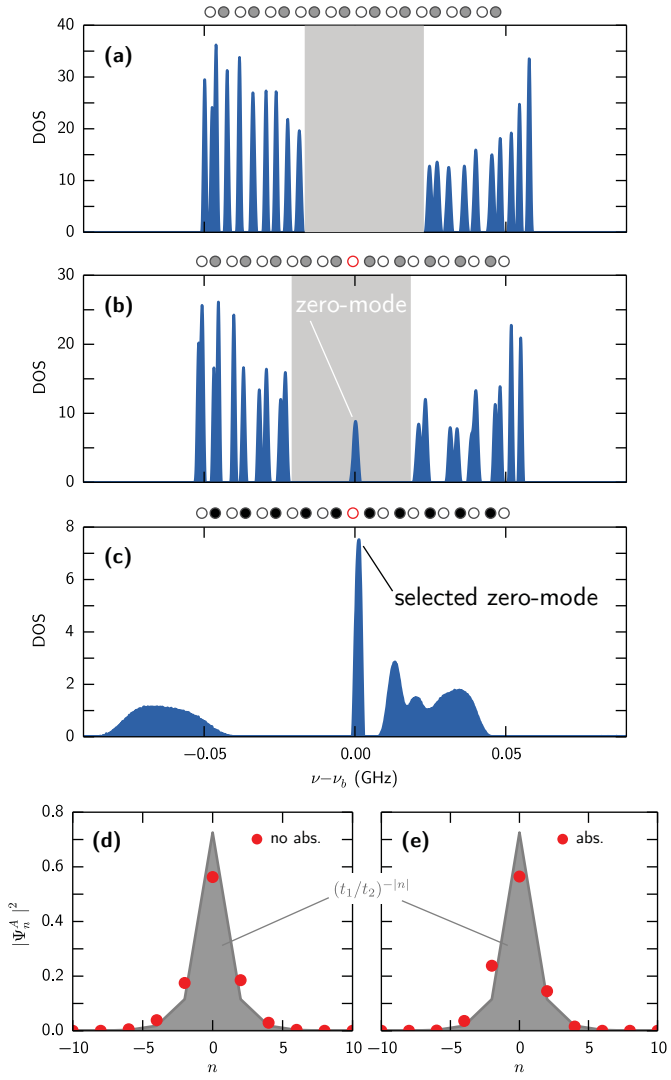
(a)
DOS
(b)
zero-mode
DOS
(c)
selected zero-mode
DOS
$\nu-\nu_b$ (GHz)
(d)
no abs.
(e)
abs.
$(t_1/t_2)^{-|n|}$
$|\Psi_n^A|^2$
n
n

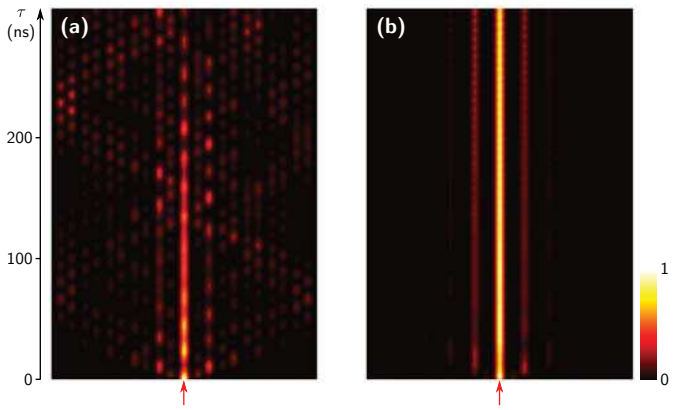
τ
(ns)
(a)
200
100
0
(b)
1
0

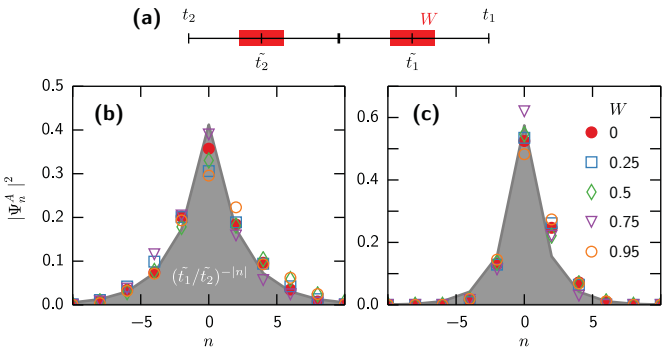
(a)
t_2
W
t_1
$\tilde{t}_2$
$\tilde{t}_1$
(b)
(c)
$|\Psi_n^A|^2$
$(\tilde{t}_1/\tilde{t}_2)^{-|n|}$
n
W
0
0.25
0.5
0.75
0.95